



Surface crack growth in cylindrical hollow specimen subject to tension and torsion

V. Shlyannikov, R. Yarullin, I. Ishtyryakov
Kazan Scientific Center of Russian Academy of Sciences
shlyannikov@mail.ru, yarullin_r@mail.ru, ivan_200999@mail.ru

ABSTRACT. The subject for studies is an aluminium cylindrical hollow specimen with external axial and part circumferential semi-elliptical surface crack undergoing fatigue loads. Both the optical microscope measurements and the crack opening displacement (COD) method are used to monitor and calculate both crack depth and crack length during the tests. The variation of crack growth behaviour is studied under cyclic axial tension, pure torsion and combined tension+torsion fatigue loading. For the particular surface flaw geometries considered, the elastic and plastic in-plane and out-of-plane constraint parameters, as well as the governing parameter for stress fields in the form of I_r -integral and plastic stress intensity factor, are obtained as a function of the aspect ratio, dimensionless crack length and crack depth. The combined effect of tension and torsion loading and initial surface flaw orientation on the crack growth for two type of aluminium alloys is made explicit. The experimental and numerical results of the present study provided the opportunity to explore the suggestion that fatigue crack propagation may be governed more strongly by the plastic stress intensity factor rather than the magnitude of the elastic SIFs alone. One advantage of the plastic SIF is its sensitivity to combined loading due to accounting for the plastic properties of the material.

KEYWORDS. Surface crack; Tension; Torsion; Crack growth.

INTRODUCTION

In order to provide operation in a safe condition, it is necessary to perform fracture mechanics assessment of a structural component under cyclic loading. The fatigue growth analysis of surface cracks is one of the most important elements for structural integrity prediction of the circular cylindrical metallic components (bars, wires, bolts, shafts, etc.) in the presence of initial and accumulated operation damages. In most cases, part-through flaws appear on the free surface of the cylinder and defects are approximately considered as semi-elliptical cracks. Multiaxial loading conditions including tension/compression, bending and torsion are typical for the circular cylindrical metallic components of engineering structures. The problem of residual fatigue life prediction of such type of structural elements is complex and the closed solution is often not available because surface flaws are three-dimensional in nature. The fatigue failure of cylindrical specimens often develops from surface flaws, and thus several analyses have been carried out to determine the stress intensity factors along the front of an edge defects and crack growth rate study on this base [1-4]. An actual surface crack may usually be replaced by an equivalent circular arc or elliptical-arc edge flaw. The elastic stress intensity factors have been published for part-circular, part-elliptical, or straight fronted cracks in a cylindrical specimen.

In this paper, firstly experimental results of fatigue crack growth for a crack starting from a semi-elliptical edge notch in an cylindrical hollow specimens under axial loading with or without cyclic torsion are given. The influence of different

loading conditions on fatigue life of cylindrical specimens is discussed. The relations of crack opening displacement and crack length on the free surface of specimens are obtained and it is shown that the growth of the crack fronts is dependent on the initial notch form. Using the aforementioned relations, the crack front shape and crack growth rate in the depth direction can be predicted. The simulations for the crack path assessment are based on the constrain parameters behaviour. The computational 3D fracture analyses deliver a governing parameter of elastic-plastic stress field distributions along the crack front. On this base crack growth interpretation is performed using the traditional elastic and new plastic stress intensity factors [5-7]. Different crack growth rate is observed in the direction of the deepest point of the crack front with respect to the free surface of the hollow cylindrical specimen.

SPECIMENS AND MATERIAL PROPERTIES

The test materials are aluminum alloys D16T and B95 which main mechanical are listed in Tab. 1 where E is the Young's modulus, σ_b is the nominal ultimate tensile strength, σ_0 is the monotonic tensile yield strength, σ_u is the true ultimate tensile strength, δ is the elongation, ψ is the reduction of area, n is the strain hardening exponent and α is the strain hardening coefficient.

Aluminum alloy	$\sigma_{0.2}$ MPa	σ_b MPa	δ %	ψ %	σ_u MPa	E GPa	n	α
D16T	439	590	9	9	645	75.922	5.88	1.5
	438	598	12	13	686	77.191	5.85	1.58
B95AT	442	604	11	11	658	77.734	5.79	1.66
	470	637	10	15	731	74.135	6.62	1.62

Table 1: Main mechanical properties of aluminum alloys.

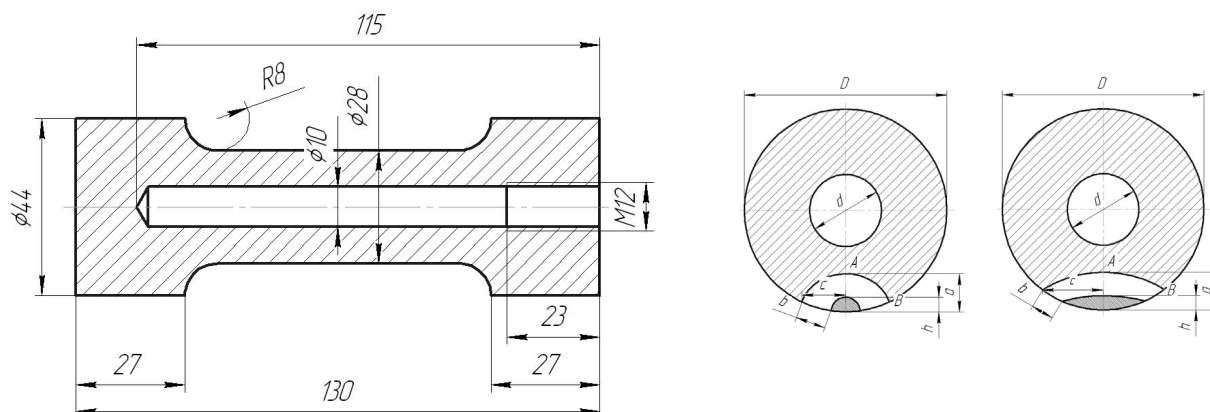


Figure 1: Details of the hollow specimen geometry and initial notches.

The hollow cylindrical specimen geometry configuration is shown in Fig. 1. The diameter is equal to 28 mm in the test section and the length is equal to 130 mm. Using linear cutting machine surface edge cracks were cut with initial flaw depths b_0 3.0 mm for both a circular arc and elliptical-arc initial edge notch. The geometric parameters of the specimen test section and of the growing crack are shown in Figs. 1 and 2. In these figures, b is the current crack depth, with the crack front approximated by an elliptical curve with major axis $2c$ and minor axis $2a$. The crack length b is obtained by measuring the distance between the advancing crack break through point and the notch break through point, as shown in Fig. 2. The depth of the initial curvilinear edge notch is denoted by a and the initial notch length by b . The crack opening displacement is measured on the free hollow specimen cylindrical surface, in the central plane of symmetry as shown in Fig. 2. The Axial Torsion Test System *Bi-00-701* is used for axial-torsional fatigue and fracture testing of the hollow cylindrical specimens. This system is equipped with: fatigue rated axial-torsional dynamic load cell with axial capacity 100 kN and torsional capacity 2 kN-m; *Bi-06-3XX* series axial extensometers and torsional strain measurement fixture. The crack length on the specimen lateral surface were monitored using the optical instrumental zoom microscope whereas, to fix the crack opening displacement of specimen at the gauge length, a pulley arrangement with an externally axial encoder



is introduced (Fig. 2). All tests are carried out with sinusoidal loading form, with load and torque moment control. For the simple cyclic tension fatigue tests, the specimens are tested with an applied maximum nominal stress equal to 80 MPa and with a frequency value 10 Hz. The combined tension/torsion tests are performed with the same stress ratio, applying synchronous and in-phase tensile and shear stresses whose maximum values are respectively equal to 75 and 59 MPa.

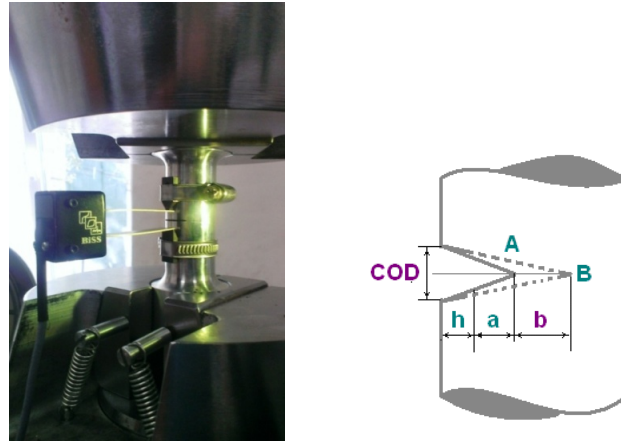
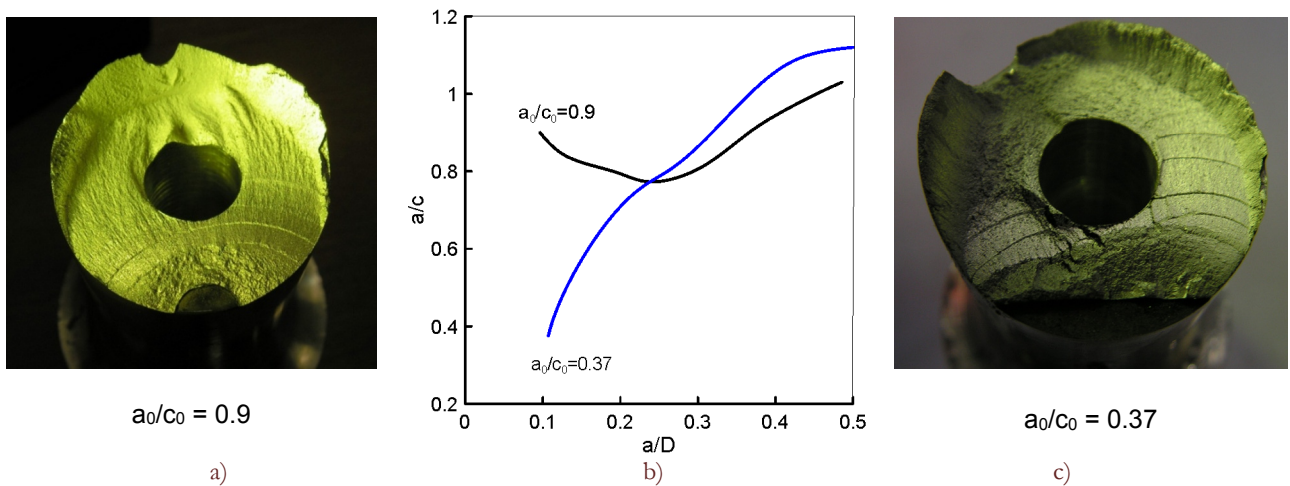
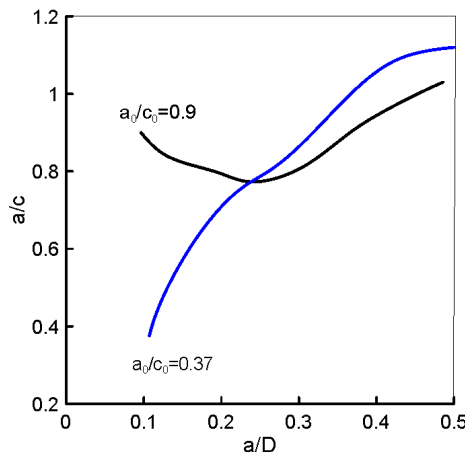


Figure 2: Test equipment for measuring COD and edge crack geometric parameters.



$a_0/c_0 = 0.9$

a)



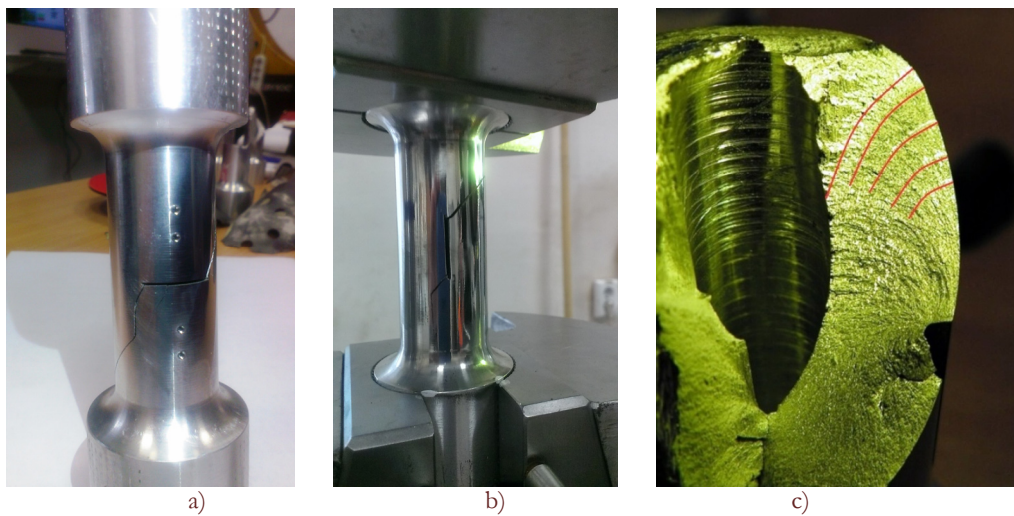
a/D

b)

$a_0/c_0 = 0.37$

c)

Figure 3: Aspect ratio versus crack depth under tension for different initial surface flaw geometries.



a)

b)

c)

Figure 4: Surface crack paths under torsion for (a) transverse and (b,c) longitudinal initial notches.



Two different stress ratio R_f values (0.1 and 0.5) were applied several times to the specimens in order to highlight the crack front geometry during propagation: during each test, beach marks were produced on each specimen by increasing the applied stress ratio from 0.1 to 0.5 at constant value of maximum cyclic nominal stress, when the surface crack length was approximately increased to $a \cong 0.1\text{mm}$. The typical beach marks on the post mortem cross section of different specimens are shown in Figs. 3 and 4 for tension and torsion, respectively. From the crack front shape obtained in this way, the relations between the relative crack depth a/D and the surface crack chord length c/D can be measured using a comparison microscope. In addition, based on periodically measured increments of surface crack chord length Δb , the curve of surface crack propagation versus cycle numbers db/dN can be obtained. Afterwards, utilizing the relation of crack depth versus surface crack chord length, it is possible to obtain the crack growth rates da/dN in the depth direction. Another interesting result pointed out in the present study is the crack front and aspect ratio stabilization (Fig.3,b) with respect to different initial notch geometry, when considering the analyzed multiaxial loading condition. It can be seen that the crack propagation paths differ with diverse initial flaw forms, but converge to the same configuration when the crack depth ratio is larger than about 0.25.

NUMERICAL RESULTS

Dimensionless coordinates

From Figs. 3 and 4 can be seen that the length of the arc of semi-elliptical crack front depends on the loading conditions of the hollow specimens. Moreover, the crack propagation process in hollow samples can be divided into two stages. During the first stage a semi-elliptical crack is a part-through-thickness. On the second stage semi-elliptical crack completely crosses the cylinder wall and becomes a through-thickness. To compare the parameter distributions along the semi-elliptical crack front is convenient to introduce the dimensionless coordinates in the following form:

$$x_0 = \Delta\varphi \cos \varphi_0, \quad y_0 = \Delta\varphi \sin \varphi_0 \tag{1}$$

$$x_c = \Delta\varphi \cos \varphi_c, \quad y_c = \Delta\varphi \sin \varphi_c$$

$$x_i = \Delta\varphi \cos \varphi_i, \quad y_i = \Delta\varphi \sin \varphi_i, \quad \varphi_i \in [\varphi_0, \varphi_c], \quad \Delta\varphi = \varphi_c - \varphi_0$$

$$\bar{X}_i = \frac{x_0 - x_i}{x_0 - x_c}; \quad \bar{Y}_i = \frac{y_i - y_0}{y_c - y_0} \tag{2}$$

$$R_i = \frac{1}{\sqrt{2}} \sqrt{\bar{X}_i^2 + \bar{Y}_i^2}, \quad R \in [0, 1] \tag{3}$$

where φ_0 is angle determining position of initial point of the semi-elliptical crack front whereas φ_c is angle corresponding to the deepest point of the crack front. In the following representation of numerical results, we will use variable R changing in the range from 0 to 1.

Constraint parameters

Recently, several two parameter models describing elastic-plastic fracture mechanics were introduced to explain some of the restrictions inherent in the one parameter approach based on the J -integral. The different sources of changes in the in-plane and out-of-plane constraint are associated with the crack size, the geometry of the specimen and the loading conditions and notch effects on the fracture resistance characteristics of structural materials. Characterization of the constraint effects in the present study was performed using the non-singular T -stresses, the local triaxiality parameter b and the T_z -factor of the stress-state in a 3D cracked body to illustrate the features of the behavior of surface cracks in the hollow specimen.

T-stress

The T -stress has been recognized to present a measure of the constraint for the small-scale yielding conditions. Few methods have been proposed for calculating T . This study explores the direct application of FEM analysis by using the crack flank nodal displacements for calculating T -stress. Using this technique, the T -stress distributions in various specimen geometries were determined from numerical calculations. To this end, the commercial finite element code, ANSYS [8], was used to calculate the stress distributions ahead of the crack tips. In this part of the FEA calculations, the material is assumed to be linear elastic and characterized by $E=74 \text{ GPa}$ and $\nu=0.3$.



T_z factor

The T_z factor [9] has been recognized to present a measure of the out-of-plane constraint and can be expressed as the ratio of the normal elastic-plastic stress components

$$T_z = \frac{\sigma_{zz}}{\sigma_{xx} + \sigma_{yy}} \tag{4}$$

where σ_{zz} is the out-of-plane stress, and σ_{xx} and σ_{yy} are the in-plane stresses. The variation of this parameter is important to characterize the thickness effect on the crack front stress distribution and the changes of the plastic zone size.

Stress triaxiality

As a secondary fracture parameter, a local parameter of the crack-tip constraint was proposed by the authors [10] because the validity of some of the above-mentioned concepts depends on the chosen reference field. This stress triaxiality parameter is described as follows:

$$h(r, \theta, z) = \sigma_{kk} / \left(3 \sqrt{\frac{3}{2} s_{ij} s_{ij}} \right) \tag{5}$$

where σ_{kk} and s_{ij} are the hydrostatic and deviatoric stresses, respectively. Being a function of both the first invariant of the stress tensor and the second invariant of the stress deviator, the stress triaxiality parameter is a local measure of the in-plane and out-of-plane constraint that is independent of any reference field.

The distributions of the elastic and elastic-plastic constraint parameters along the crack front in the hollow specimen under cyclic tension are plotted in Fig. 5 under pure Mode I loading. These distributions correspond to the crack front positions at the accumulated number of loading cycles $N_1=0$ (initial front), $N_2= 21000$ (intermediate front), $N_3= 50000$ (intermediate front), $N_4= 131500$ (final failure front). The constraint parameter is plotted against the normalized coordinate R . In this plot $R = 0.0$ is the crack border (the specimen free surface) while $R = 1.0$ is the mid-plane of the hollow specimen thickness. It can be observed that all constraint parameters essentially changed along the crack front from the free surface toward the mid-plane. It should be noted that the front of the number four in the Fig. 5 corresponds to the second stage of crack propagation when it becomes completely through-thickness and intersects the cylinder wall.

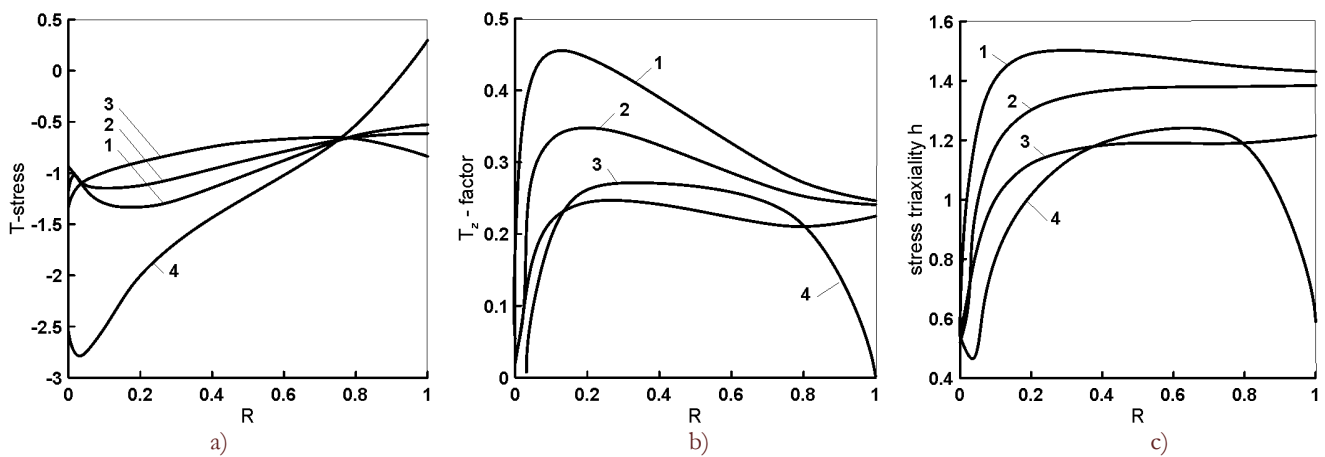


Figure 5: Constraint parameter distributions under cyclic tension along crack front (1-initial, 2-3-intermediate, 4-final).

Plastic stress intensity factor

Here, our primary interests are to obtain an accurate description for the distribution along the crack front of the governing parameter for the elastic-plastic solution in the form of an I_n -integral and to determine the accuracy that this type of calculation, which will later be used for the general 3D problem, provides for the plastic stress intensity factor (SIF). The method developed here for combining the knowledge of the dominant singular solution with the finite element technique to obtain accurate solutions in the neighborhood of a crack tip is also applicable to the treatment of problems involving cracks in finite bodies.



In accordance with the approach of Hutchinson [11], the plastic stress intensity factor K_p in pure Mode I (or pure Mode II) can be expressed directly in terms of the corresponding elastic stress intensity factor using Rice's J -integral. That is

$$J = \frac{(K_1^2)}{E'} = \frac{\bar{\alpha}\sigma_0^2}{E'} I_n(\theta) (K_p)^{n+1}; \quad (6)$$

$$\bar{K}_p = \left[\frac{(\bar{K}_1^2)}{\bar{\alpha}\sigma_0^2 I_n(\theta)} \right]^{1/(n+1)} = \left[\left(\frac{\sigma}{\sigma_0} \right)^2 \frac{\pi\lambda Y_1^2(a/w)}{\bar{\alpha} I_n(\theta)} \right]^{1/(n+1)}; \quad \bar{K}_1 = \sigma\sqrt{\pi\lambda} \cdot Y_1(a/w) \quad (7)$$

where $\bar{K}_1 = K_1/\sqrt{w}$ is normalized by a characteristic size of cracked body elastic stress intensity factor and $E' = E$ for plane stress and $E' = E/(1-\nu^2)$ for plane strain. In the above equations, $\bar{\alpha}$ and n are the hardening parameters, $\lambda = a/w$ is the dimensionless crack length, w is characteristic size of specimen (for our case that is specimen diameter), σ is the nominal stress, and σ_0 is the yield stress. The numerical constant $I_n(\theta)$ is obtained from the singularity analysis by means of the conjugation solutions for the far and near fields. For small-scale yielding, i.e., when the plastic zone near the crack tip is quite small compared with the crack length, the amplitude of the singularity \bar{K}_p can be determined directly by application of the J -integral. In the framework of the present work, the conditions at the crack tip are described using the J -integral and an inherent parameter I_n that must be determined for the tested hollow specimens as well as for the structural elements to enable the applicability of the results. To address the theoretical aspects relevant to the experiments, finite element analysis is used to determine the governing parameter I_n of the asymptotic behavior of the stresses at the crack tip.

In the classical first-term singular HRR-solution [11], the numerical parameter I_n is a function of only the material strain hardening exponent n . Shlyannikov and Tumanov [5] reconsidered the HRR-solution for both plane strain and plane stress and supposed that under small-scale yielding, the expression for I_n depends implicitly on the dimensionless crack length and the specimen configuration. In this section, we extend the analysis to the I_n -integral behavior in an infinitely sized cracked body [11] to treat the test specimen's specified geometries. The use of the Hutchinson's theoretical definition for the I_n -factor directly adopted in the numerical finite element analyses leads to [5]

$$I_n^{FEM}(\theta, M_p, n, (a/w)) = \int_{-\pi}^{\pi} \Omega^{FEM}(\theta, M_p, n, (a/w)) d\theta \quad (8)$$

$$\Omega^{FEM}(\theta, M_p, n, (a/w)) = \frac{n}{n+1} (\tilde{\sigma}_e^{n+1})^{FEM} \cos\theta - \left[\tilde{\sigma}_r^{FEM} \left(\tilde{u}_\theta^{FEM} - \frac{d\tilde{u}_r^{FEM}}{d\theta} \right) - \tilde{\sigma}_{r\theta}^{FEM} \left(\tilde{u}_r^{FEM} + \frac{d\tilde{u}_\theta^{FEM}}{d\theta} \right) \right] \sin\theta - \frac{1}{n+1} (\tilde{\sigma}_r^{FEM} \tilde{u}_r^{FEM} + \tilde{\sigma}_{r\theta}^{FEM} \tilde{u}_\theta^{FEM}) \cos\theta.$$

In this case, the numerical integral of the crack tip field I_n changes not only with the strain hardening exponent n but also with the relative crack length b/D and the relative crack depth a/D . More details to determine the I_n factor for different test specimen configurations are given by Refs. [5-7].

The distribution of the elastic-plastic constraint parameters along the crack front in the direction from the free surface toward the mid-plane is plotted in Fig. 6 for the hollow specimens under different loading conditions. The left picture in Fig. 6 depicts the behavior of the I_n -factor, whereas the right picture in Fig. 6 gives us the distribution of the stress triaxiality parameter b for the fixed curvilinear crack front position. The constraint parameters are plotted against the normalized coordinate R . In these plots $R = 0.0$ is the crack border (the specimen free surface) while $R = 1.0$ is the mid-plane of the specimen. It can be observed from these figures that both constraint parameters sufficiently changed along the crack front from the free surface toward the mid-plane as a function of loading conditions. Fig. 7 represents the distributions of the I_n -factor for the pure tension and pure torsion as well as the combined loading conditions for different crack front position in hollow specimens.

The last part of the numerical calculations of the present study is devoted to the determination of the plastic stress intensity factors in hollow samples. In Fig.8 shown the distributions of the elastic and plastic SIF's for the same tensile loading conditions along the same crack front. Fig. 8 gives a clear illustration of the necessity to take into account the



plastic properties of the material in the interpretation of the characteristics of the material resistance to crack propagation. The data shown in Fig. 9 confirm this suggestion in more details for several other crack fronts. Recall that the front of the number four in the Fig. 9 corresponds to the second stage of crack propagation when it becomes completely through-thickness and intersects the hollow cylinder wall.

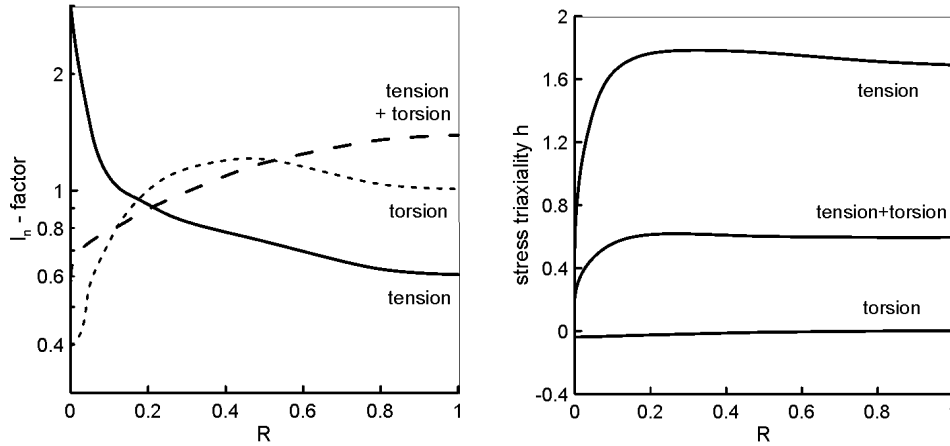


Figure 6: I_n -factor and stress triaxiality parameter distributions along crack front under different loading conditions.

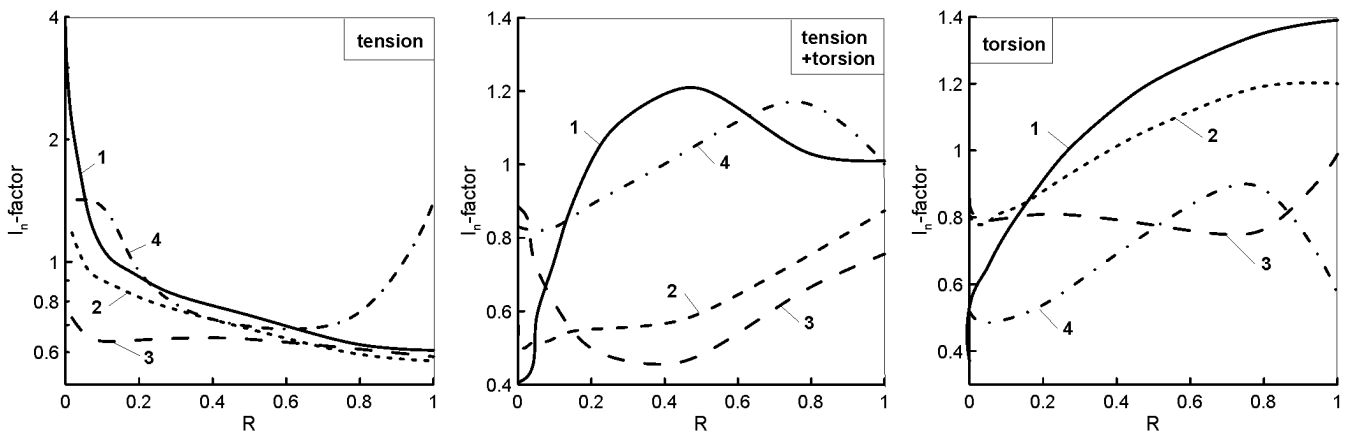


Figure 7: I_n -factor distributions along crack front under different loading conditions (1-initial, 2-3-intermediate, 4-final crack front).

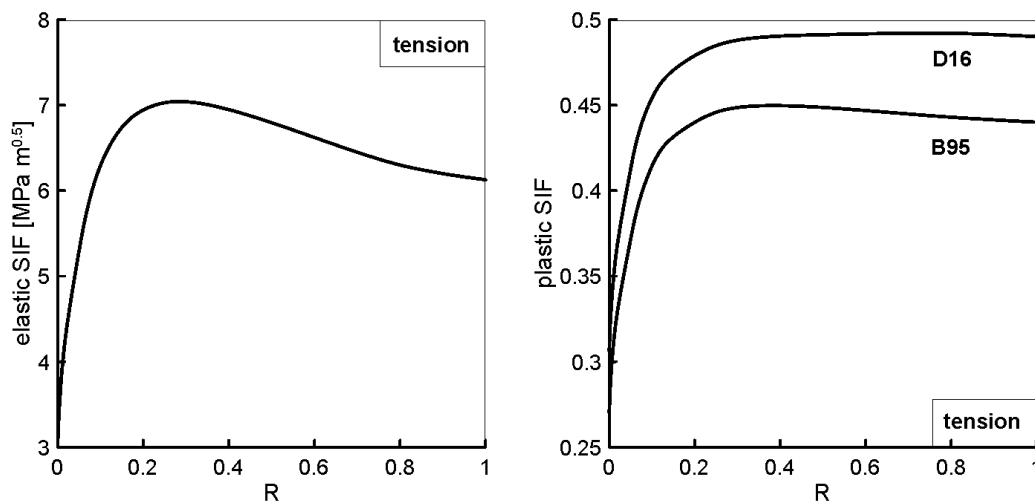


Figure 8: Elastic and plastic stress intensity factor behavior for initial crack front under tension.

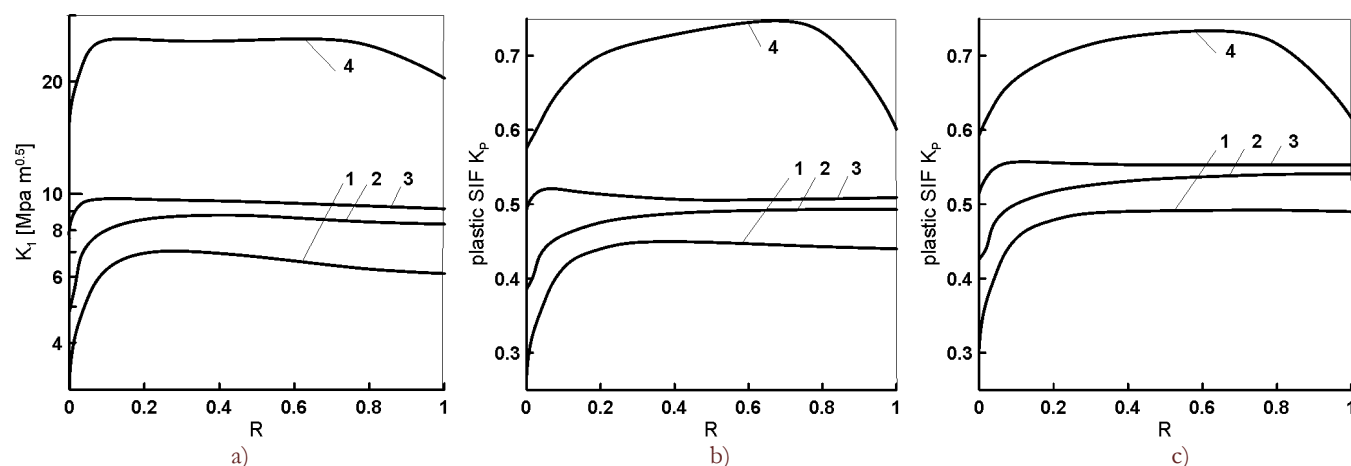


Figure 9: Elastic (a) and plastic stress intensity (b-B95, c-D16) factor distributions along crack front (1-initial, 2-3-intermediate, 4-final).

EXPERIMENTAL RESULTS AND DISCUSSION

The evolution of the crack growth rate of the elliptical-fronted edge cracks during the tests is determined using COD and the microscope. In order to study the crack growth under fatigue tension loading with superimposed cyclic torsion, several hollow specimens of both aluminum alloys B95 and D16 are tested with an initial notch depth equal to 3 mm. Fig. 10 shows plot of the break through point advances b and of COD against the number of cycles N under pure tension and combined loads, respectively. As shown in Fig. 10, in-phase cyclic torsion loading superimposed on cyclic tension leads to different effects on the relationship between crack length on the free surface of the specimen and crack opening displacement under combined cyclic loading which depend on the material properties. Nevertheless there is a strong correlation between these two parameters that can be very useful for automation of experimental studies of fatigue and fracture under multiaxial stress state. On the base of this experimental data, polynomial functions can be used to express the COD as a function of the superficial crack length.

Fig. 11 represents the superficial crack growth rate db/dN versus COD on the hollow cylindrical specimens undergoing pure tension and combined loading. It is found that the crack growth rate along the external surface direction as a function of COD fit into a single curve with a small scatter band of the experimental results under different loading conditions for both tested aluminum alloys. However, looking at Figs.3,4 and considering changes in the general durability of the specimens in pure tension and combined loading, significant differences in the crack growth rate in the depth direction a and on the free surface b of hollow specimens under the above types of loading conditions are expected.

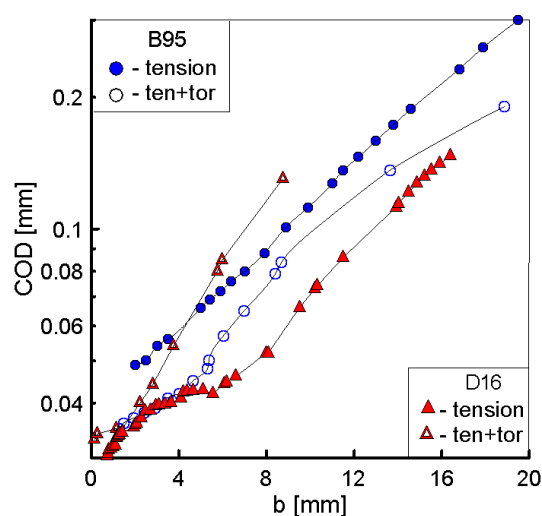


Figure 10: Relationship between COD and crack length on free surface of hollow specimen under different loading conditions.

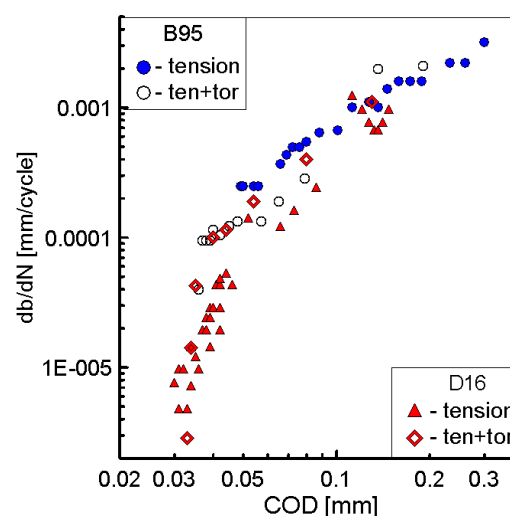


Figure 11: Crack growth rate on free surface of hollow specimen versus COD under different loading conditions.



Fig. 12 shows the typical experimental fatigue fracture diagrams in the coordinates of the crack growth rate versus the values of the stress intensity factors for the hollow cylindrical specimens tested under pure tensile loading. The left picture in Fig. 12 depicts the behavior of the db/dN as a function of the elastic SIF K_I , whereas the right picture in Fig. 12 gives us the crack growth rate depending on of the dimensionless plastic stress intensity factor K_p . To determine the experimental values of the elastic and plastic SIF's for two main points of the crack front, namely, the free surface and midplane section, was used the distributions represented in Fig. 9. Looking at Fig.12 it should be noted that increasing of the crack growth rates is observed in the direction of the deepest point of the crack front with respect to the crack front intersection with the free surface of the hollow cylindrical specimens in terms of the elastic and plastic SIF's.

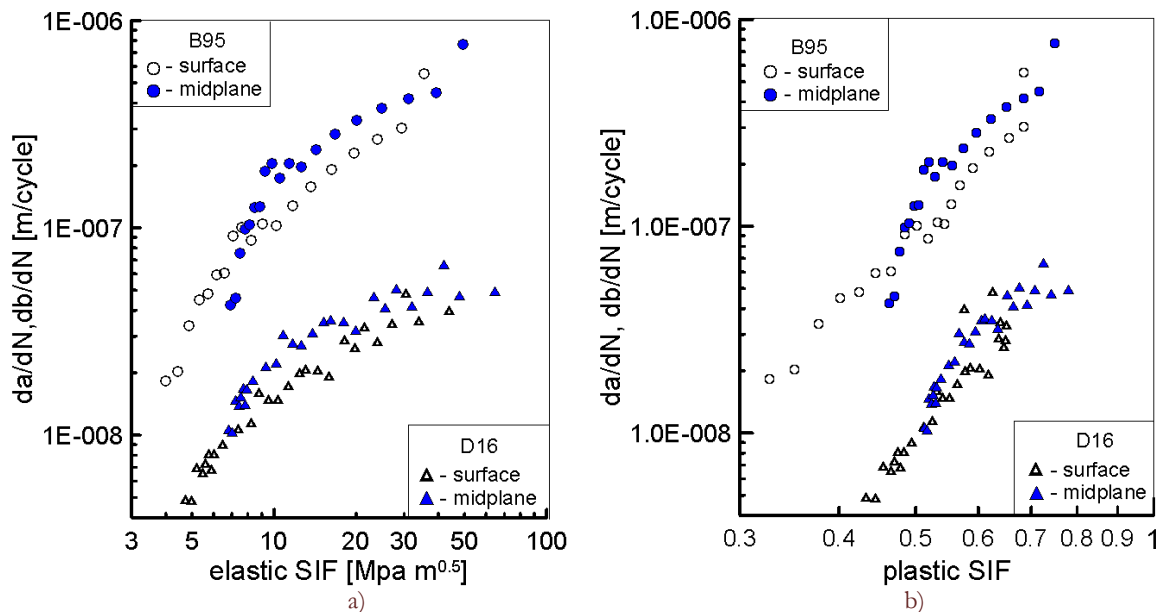


Figure 12: Crack growth rate as a function of (a) elastic and (b) plastic SIFs under tension for different crack front points.

In contrast to the elastic SIF K_I , the plastic SIF K_p shows very useful effect of the sensitivity to the plastic properties of the tested materials. It can be seen from Fig. 12 that the plastic SIF gradually increases by increasing the crack length and crack depth at fixed elastic properties of the aluminum alloys characterized by $E=74$ GPa and $\nu=0.3$. The data presented very obvious advantages of using the plastic stress intensity factors to characterize the material's resistance to cyclic crack growth. This conclusion is confirmed by the relative position of crack growth curves in Fig.12 for both tested aluminum alloys under pure cyclic tension in the terms of the elastic and plastic SIF's.

CONCLUSIONS

Fatigue crack growth for an elliptical arc-fronted edge crack with two different initial notch form in hollow cylindrical specimens of B95 and D16 aluminum alloys is studied. Experiments and calculations made under axial cyclic tension with and without cyclic torsion are described. All the experimental and numerical results are shown:

- for the same specimen configuration and different the crack front position as a function of cyclic tension and torsion loading, the following constraint parameters were analysed, namely, the non-singular T -stress, T_ζ -factor and the stress triaxiality parameter b in the 3D series of elastic-plastic computations for aluminum alloys different properties;
- the governing parameter of the elastic-plastic stress fields I_n -factor distributions along various crack fronts was also determined from numerical calculations, this governing parameter is used as the foundation of the elastic-plastic stress intensity factor;
- under pure cyclic tension loading, it can be seen that the crack propagation paths differ with diverse initial flaw forms, but converge to the same configuration when the crack depth ratio is larger than about 0.25;
- it is found that there is one general relationship between the crack growth rate on the free surface of specimen and COD for both tested aluminum alloys and loading conditions including the case when the torsion loading is superimposed on the cyclic tension;



- increasing of the crack growth rates is observed in the direction of the deepest point of the crack front with respect to the crack front intersection with the free surface of the hollow cylindrical specimens;
- the experimental and numerical results of the present study background provide an opportunity to explore the suggestion that crack growth rate may be represented by the plastic stress intensity factor, rather than the magnitude of the elastic SIFs alone;
- it is stated that the elastic-plastic stress intensity factor, which is sensitive to the constraint effects and elastic-plastic material properties, is attractive as the self-dependent unified parameter for characterization of the material fracture resistance properties.

ACKNOWLEDGMENT

The authors gratefully acknowledge the financial support of the Russian Scientific Foundation under the Project 14-19-01716.

REFERENCES

- [1] Newman, J.C., Raju, I.S., An empirical stress-intensity factor equation for the surface crack, *Eng. Fract. Mech.*, 15 (1-2) (1981) 185-192.
- [2] Carpinteri, A., Brighenti, R., Part-through cracks in round bars under cyclic combined axial and bending loading, *Int. J. Fatigue*, 18 (1) (1996) 33-39.
- [3] Yang, F.P., Kuang, Z.B., Shlyannikov, V.N., Fatigue crack growth for straight-fronted edge crack in a round bar, *Int. J. Fatigue*, 28 (2006) 431-437.
- [4] Citarella, R., Lepore, M., Shlyannikov, V., Yarullin, R., Fatigue surface crack growth in cylindrical specimen under combined loading, *Eng. Fract. Mech.*, 131 (2014) 439-453.
- [5] Shlyannikov, V.N., Tumanov, A.V., Characterization of crack tip stress fields in test specimens using mode mixity parameters, *Int. J. Fract.*, 185 (2014) 49-76.
- [6] Shlyannikov, V.N., Zakharov, A.P., Multiaxial crack growth rate under variable T-stress, *Eng. Fract. Mech.*, 123 (2014) 86-99.
- [7] Shlyannikov, V.N., Tumanov, A.V., Zakharov, A.P., The mixed mode crack growth rate in cruciform specimens subject to biaxial loading, *Theoret. Appl. Fract. Mech.*, 73 (2014) 68-81.
- [8] ANSYS Mechanical APDL Theory Reference Release 14.5// ANSYS, Inc. Southpointe, 275 Technology Drive, CanonBurg, PA 2012.
- [9] Guo, W.L., Elasto-plastic three dimensional crack border field-I, *Eng. Fract. Mech.*, 46 (1993) 93-104.
- [10] Henry, B.S., Luxmoore, A.R., The stress triaxiality constraint and the Q-value as ductile fracture parameter, *Eng. Fract. Mech.*, 55 (1997) 375-390.
- [11] Hutchinson, J.W., Singular behaviour at the end of a tensile crack in a hardening material, *Journ. Mech. Phys. Solids*, 16 (1968) 13-31.